Retroactivity attenuation through signal transduction cascades

Phillip M. Rivera[1] and Domitilla Del Vecchio[1]

Abstract— **This paper considers the problem of attenuating retroactivity, that is, the effect of loads in biological networks and demonstrates that signal transduction cascades incorporating phosphotransfer modules have remarkable retroactivity attenuation ability. Uncovering the biological mechanisms for retroactivity attenuation is relevant in synthetic biology to enable bottom-up modular composition of complex circuits. It is also important in systems biology for deepening our current understanding of natural principles of modular organization. In this paper, we perform a combined theoretical and computational study of a cascade system comprising two phosphotransfer modules, ubiquitous in eukaryotic signal transduction, when subject to load from downstream targets. Employing singular perturbation on the finite time interval, we demonstrate that this system implements retroactivity attenuation when the input signal is sufficiently slow. Employing trajectory sensitivity analysis about nominal parameters that we have identified from *in vivo* data, we further demonstrate that the key parameters for retroactivity attenuation are those controlling the timescale of the system.**

I. Introduction

The description of biomolecular circuits through functional modules [1] relates cellular biology to synthetic disciplines such as computer science and engineering. Modularity is the property that allows the assembly of larger system through the use of units that perform independently (modules) as building blocks [2]. Yet, the predictable and functional composition of complex systems from simpler modules still remains one of the challenges in synthetic biology [3][4]. One problem lies in the presence of an impedance-like effect known as retroactivity, which creates context dependencies that change the internal state of the individual modules upon interconnection [5][6][7].

It has been demonstrated *in vivo* that retroactivity can affect the level of MAPK (mitogen-activated protein kinase) phosphorylation depending on substrate concentration [8]. It has also been reported that retroactivity can change the response time of a uridylyltransferase/uridylyl-removing enzyme (UTase/UR)–PII system [9], and induce time delays in gene transcription networks [10], thus affecting the dynamic behavior of biomolecular systems. To attenuate retroactivity effects, which can disrupt a module functionality, the implementation of insulation devices was proposed [6][11]. The behavior of an insulation device is similar to that of a non-inverting amplifier, which buffers the dynamics of the upstream circuit from the impedance effects due to downstream load. Similarly, the insulation device allows for the preservation of the temporal behavior of the interconnected modules by mitigating retroactivity effects upon interconnection.

Jayanthi et al. [11] provide a formal mathematical treatment of systems with the retroactivity attenuation property employing the principle of timescale separation. This principle states that if the insulation device internal dynamics are on a much faster timescale compared to the input timescale, the output presents no tracking error even in the presence of high load. The main result, based on Tikhonov's theorem of singular perturbation [on the finite time interval [12], suggests that the fast internal dynamics of the insulation device allows the system trajectories to immediately approach a (asymptotically stable) slow manifold. This manifold, in turn, can be made independent from the load when key regulatory elements are in sufficiently large amounts.

This work presents the analysis of an insulation device realization based on the natural YPD1/SKN7 phosphotransfer cascade in *Saccharomyces cerevisiae*. The YPD1/SKN7 pathway is part of a phosphorelay circuit of the osmotic stress response mechanism in yeast [13]. It consists of a series of phosphotransfer reactions with timescale in the sub seconds range, ideal to provide the fast internal dynamics of the insulation device. Thus, it is our goal to show that the fast nature of the phosphotransfer reactions indeed allow for the successful operation of the insulation device based on timescale separation.

This paper is organized as follows. Section II mathematically characterizes a class of systems that have the retroactivity attenuation property through timescale separation. In Section III, the mathematical model formulation of a specific YPD1/SKN7 pathway realization is presented. It also shows how the YPD1/SKN7 system fits this class of systems described in Section II, thus possessing the retroactivity attenuation property. A parameter sensitivity analysis on the insulation devices output error is provided in Section IV, while Section V describes the dependence of the output error on phosphorylation timescale and total concentration of key regulatory elements which are the physical tunable parameters of the system.

II. Retroactivity attenuation

An interconnection diagram of two general biomolecular systems is presented in Fig. 1. Here, the arrows traveling in the rightward direction model the information carrier signals, while arrows traveling in the leftward direction model retroactivity signals, a scheme first introduced in Del Vecchio et. al. [6]. System Σ has input signals u and s, and output signals y and r. The internal state x of system Σ is

This work was supported by grant #FA9550-12-1-0219 and #NSF-CCF-1058127

[1]Mechanical Engineering Department, Massachusetts Institute of Technology, 77 Mass. Ave, Cambridge MA. pmrivera@mit.edu

dependent on input u and retroactivity to the output s, while applies a retroactivity to the input signal r in its upstream system. System Ω has input y, output s, and internal state v. It applies retroactivity s to system Σ.

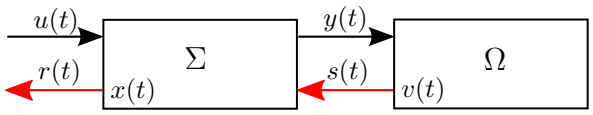

Fig. 1: System Σ transmits input signal u to the output y while its internal state x is subjected to retroactivity to the output s. System Ω with internal state v has y as an input and applies the retroactivity to the output signal s to Σ.

We can claim system Σ is an insulation device if it possesses the following properties.

Definition 1. System Σ has *small retroactivity to the input* if the retroactivity r is close to zero. That is, there is a $\rho > 0$ independent of ζ such that $\|r\| \leq \rho\zeta$, where ζ can be made arbitrarily small.

Definition 2. System Σ has the *retroactivity to the output attenuation property* if the effect of retroactivity s on the internal state x is attenuated. That is, there is a k independent of ξ such that $\|x(t,s) - x(t,0)\| \leq k\xi$ for all t, where ξ can be made arbitrarily small.

Definition 3. System Σ is called an *insulation device* if it has both small retroactivity to the input and the retroactivity to the output attenuation property.

The following theorem introduces a specific class of systems Σ that employ the principle of timescale separation for retroactivity to the output attenuation.

Theorem 1. Consider system Σ

$$\dot{u} = g(t,u), \tag{1}$$
$$\epsilon\dot{x} = f(u,x,\epsilon_1\psi(v)) + \epsilon M s(y,v), \tag{2}$$
$$y = Cx, \tag{3}$$
$$\dot{v} = Bs(y,v) + h(y,v), \tag{4}$$

where $\|\psi(v)\| \leq a$, C, B and M are constant matrices, $0 < \epsilon \ll 1$ is a singular perturbation parameter and $0 < \epsilon_1 \ll 1$ is a small constant parameter. Let the following assumptions hold for $t \in [t_0, t_1]$:

1) For $f(u,x,\epsilon_1\psi(v)) = 0$ there exists a unique global mapping $x = \gamma(u,\epsilon_1\psi(v))$ and for $f(u,x_0,0) = 0$ there is a unique global mapping $x_0 = \gamma_0(u)$.
2) Functions f, g, s and h are smooth on all parameters.
3) The slow system $\dot{u} = g(t,u)$, $\dot{v} = Bs(C\gamma(u,\epsilon_1\psi(v)),v) + h(C\gamma(u,\epsilon_1\psi(v)),v)$ has a unique solution $(u(t), \bar{v}(t,\epsilon_1))$.
4) System $\frac{dx}{d\tau} = f(u,x,\epsilon_1\psi(\bar{v}))$, where $\tau = t/\epsilon$ and u, $\bar{v}$, t are frozen in time, has a locally exponentially stable equilibrium point $\bar{x}$ uniformly in $(u, \epsilon_1\psi(\bar{v}))$, with $x(t_0)$ inside region of attraction of $\bar{x}$.

Then, the solution $x(t,\epsilon,\epsilon_1)$ of system (1) - (4) can be approximated by $x_0 = \gamma_0(u)$, with an error given by:

$$\|x(t,\epsilon,\epsilon_1) - \gamma_0(u)\| = O(\epsilon) + O(\epsilon_1). \tag{5}$$

Proof. Assumptions 1) - 4) allow the application of the singular perturbation theorem (Theorem 11 of Khalil [12]) which implies that there exists a constant ϵ^* such that for any initial condition inside the region of attraction of the equilibrium $\bar{x}$ of system $\frac{dx}{d\tau} = f(u,x,\epsilon_1\psi(v))$ for a time $t_b > t_0$ and $0 \leq \epsilon \leq \epsilon^*$ the singular perturbation problem (1) - (4) has a unique solution $(u(t), x(t,\epsilon,\epsilon_1), v(t,\epsilon,\epsilon_1))$ and

$$v(t,\epsilon,\epsilon_1) - \bar{v}(t,\epsilon_1) = O(\epsilon) \tag{6}$$
$$x(t,\epsilon,\epsilon_1) - \gamma(t,\epsilon_1\psi(\bar{v})) = O(\epsilon). \tag{7}$$

Furthermore, from assumption 2) we have that f is at least of class C^1. It follows from the Implicit Function Theorem [14] that the implicit function $\gamma(u,\epsilon_1\psi(v))$, such that $f(u,\gamma(u,\epsilon_1\psi(v))) = 0$, is of class C^1. From the Mean Value Theorem [14] we now have that there exists a $K > 0$ such that $\|\gamma(u,\epsilon_1\psi(v)) - \gamma(u,0)\| \leq K\|\epsilon_1\psi(v)\|$ for all v making

$$\|\gamma(u,\epsilon_1\psi(\bar{v})) - \gamma_0(u)\| \leq K\epsilon_1 a. \tag{8}$$

Now using the triangular inequality we have $\|x(u,\epsilon,\epsilon_1) - \gamma(u,\epsilon_1\psi(\bar{v})) + \gamma(u,\epsilon_1\psi(\bar{v})) - \gamma(u,0)\| \leq \|x(u,\epsilon,\epsilon_1) - \gamma(u,\epsilon_1\psi(\bar{v}))\| + \|\gamma(u,\epsilon_1\psi(\bar{v})) - \gamma(u,0)\|$. From the definition of $\gamma_0(u)$ in Assumption 1) and using results (8) - (7) yields (5). □

Remark 1. The specific class of system Σ introduced in Theorem 1 is a special instance of an insulation device in which the retroactivity to the input $r = 0$. This can be seen from Definition 3 since $r = 0$ and parameters ϵ, $\epsilon_1 \ll 1$ make $\|x(t,s) - x(t,0)\| \approx 0$.

Remark 2. Having $\epsilon \ll 1$ means that the insulation device dynamics are much faster than both upstream and downstream systems, thus the system employs timescale separation for retroactivity attenuation. This result is an extension of Jayanthi et al. [11] since we now consider the attenuation of the effect of load vector v on the insulation device's slow manifold by having $\epsilon_1 \ll 1$.

III. Problem Formulation and System Model

We will demonstrate that the natural phosphotransfer cascade realized by the YPD1/SKN7 pathway [13] can function as an insulation device attenuating the retroactivity effects due to loading. Specifically, we will show that the YPD1/SKN7 satisfies Theorem 1, thus implements the principle of timescale separation for retroactivity attenuation. Then we will identify the key biochemical parameters controlling its retroactivity attenuation property.

A. YPD1/SKN7 system reactions and model

Using the YPD1/SKN7 pathway, an insulation device was realized and experimentally validated *in vivo* [15]. We refer to this experimental realization as the YPD1/SKN7 system, and the reactions considered in its model are as follows.

First note that in this description the asterisk notation (*) will denote phosphorylation and for a species Y its italic *Y* represents its concentration. The notation considered for the YPD1/SKN7 system species is: Z represents protein STAT5, W represents protein YPD1 and X represents protein SKN7. A diagram of the YPD1/SKN7 system is given in Fig. 2, which describes the SKN7 activation pathway used in Deepak *et al.* [15]. The signal $k(t)$, illustrated as theYPD1/SKN7 system input in Fig. 2, leads to the production of protein Z which phosphorylates to form protein Z*. At the same time, Z* phosphorylates W into W*, while Z dephosphorylates W* into W. W* double phosphorylates X into X* and X** while W is able to dephosphorylate both activated forms of X. Both, X* and X** can bind to the downstream system as in Fig. 2. This downstream system consists of DNA binding sites p, but only the bound X** leads to transcriptional activation. Complexes C* and C** denote the bound form of X* and X** respectively, which can also be phosphorylated by W* and dephosphorylated by W. The decay of both Z and Z* as well as the spontaneous dephosphorylation of all phosphorylated species was considered.

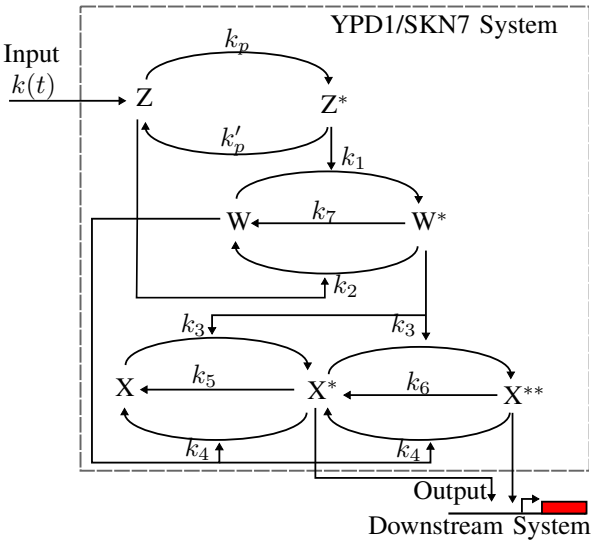

Fig. 2: YPD1/SKN7 System reactions [15]. In this diagram Z = STAT5, W = YPD1 and X = SKN7. The induction by $k(t)$ leads to the activation of output X* and X**, while X** is the only species that can lead to transcriptional activation when bound to the downstream component

A one-step reaction model of the YPD1/SKN7 System is given by the following reactionts. First, the production and decay of Z is given by: $\emptyset \xrightarrow{k(t)}$ Z , Z* $\xrightarrow{\delta} \emptyset$, Z $\xrightarrow{\delta} \emptyset$. The phosphotransfer reactions are given by: Z $\underset{k'_p}{\overset{k_p}{\rightleftharpoons}}$ Z*, Z*+W $\underset{k_2}{\overset{k_1}{\rightleftharpoons}}$ Z+W*, X+W* $\underset{k_4}{\overset{k_3}{\rightleftharpoons}}$ X*+W, X*+W* $\underset{k_4}{\overset{k_3}{\rightleftharpoons}}$ X**+W, C*+W* $\underset{k_{10}}{\overset{k_9}{\rightleftharpoons}}$ C**+W, C*+W $\xrightarrow{k_{12}}$ W*+X+p. The spontaneous dephosphorylation of phosphorylated species is given by: X* $\xrightarrow{k_5}$ X, X** $\xrightarrow{k_6}$ X*, W* $\xrightarrow{k_7}$ W, C** $\xrightarrow{k_8}$ C*, C* $\xrightarrow{k_{11}}$ X + p. And the binding/unbinding of X*, X** to DNA promoter sites p is given by: X*+p $\underset{k_{\text{off}}}{\overset{k_{\text{on}}}{\rightleftharpoons}}$ C*, X**+p $\underset{k_{\text{off}}}{\overset{k_{\text{on}}}{\rightleftharpoons}}$ C**. Defining the total Z concentration as $Z_T := Z + Z^*$, the described reactions lead to the following system of equations:

$$\dot{Z}_T = k(t) - \delta Z_T \tag{9}$$

$$\dot{Z}^* = -k_1 Z^*(W_T - W^*) + k_2 W^*(Z_T - Z^*) + k_p(Z_T - Z^*) - k'_p Z^* - \delta Z^* \tag{10}$$

$$\dot{W}^* = (k_1 Z^* + k_4 X^* + k_4 X^{**})(W_T - W^*) - k_2 W^*(Z_T - Z^*) - k_7 W^* - k_3 \left(X_T - X^{**} - C^* - C^{**}\right) W^* \overbrace{-k_9 C^* W^* + (k_{10} C^{**} + k_{12} C^*)(W_T - W^*)}^{s_1} \tag{11}$$

$$\dot{X}^* = k_3 \left(X_T - 2X^* - X^{**} - C^* - C^{**}\right) W^* + (k_4 X^{**} - k_4 X^*)(W_T - W^*) - k_5 X^* + k_6 X^{**} \overbrace{-k_{\text{on}} X^*(p_T - C^* - C^{**}) + k_{\text{off}} C^*}^{s_2} \tag{12}$$

$$\dot{X}^{**} = k_3 X^* W^* - k_4 X^{**}(W_T - W^*) - k_6 X^{**} \overbrace{-k_{\text{on}} X^{**}(p_T - C^* - C^{**}) + k_{\text{off}} C^{**}}^{s_3} \tag{13}$$

$$\dot{C}^* = k_{\text{on}} X^*(p_T - C^* - C^{**}) - k_{\text{off}} C^* + k_8 C^{**} - k_9 C^* W^* - k_{11} C^* + (k_{10} C^{**} + k_{12} C^*)(W_T - W^*) \tag{14}$$

$$\dot{C}^{**} = k_{\text{on}} X^{**}(p_T - C^* - C^{**}) - k_{\text{off}} C^{**} - k_8 C^{**} + k_9 C^* W^* - k_{10} C^{**}(W_T - W^*), \tag{15}$$

with the conservation laws: $X_T = X + X^* + X^{**} + C^* + C^{**}$, $W_T = W + W^*$, $p_T = C^* + C^{**}$, and all rate parameters as defined in the corresponding reactions. This model fits the box description presented in Fig. 1 by setting $u = Z_T$, the insulation device state vector $x = (Z^*, W^*, X^*, X^{**})^T$ and the output vector $y = (W^*, X^*, X^{**})^T$. The retroactivity to the input r is zero since Z_T is independent of all downstream processes, and the retroactivity to the output s is given by the terms under braces s_i. The internal dynamics of system Σ are given by equations (9) through (13) while the downstream system Ω with state vector $v = (C^*, C^{**})^T$ has internal dynamics given by equations (14) and (15).

B. YPD1/SKN7 retroactivity attenuation property

To see how system (9) - (15) fits Theorem 1, let us write a nondimensional version of the system and make the separation of timescale explicit by including a singular perturbation parameter ϵ. All concentrations in (9) - (15) can be normalized by their maximum value. We can define these non-dimensional concentrations as $x^* := \frac{X^*}{X_T}$, $x^{**} := \frac{X^{**}}{X_T}$, $w^* := \frac{W^*}{W_T}$, $z_T := \frac{Z_T}{Z_0}$, $z^* := \frac{Z^*}{Z_0}$, $c^* := \frac{C^*}{p_T}$, $c^{**} := \frac{C^{**}}{p_T}$, where Z_0 is the maximum concentration Z_T can reach and it is given by $Z_0 := \max_t k(t)/\delta$. This makes the range of all states $[0, 1]$ for all time. From this non-dimensional model we can see that the timescale of the z_T differential equation is given by the decay rate $\delta \in [0.004, 0.01]$ min^{-1} [16], but the remaining differential equations evolve in a faster timescale determined by phosphotransfer reactions. We consider, specifically, that all reactions involving kinetic rates $\{k_p, W_T k_1, W_T k_2, W_T k_3, W_T k_4, k_6\}$ as evolving in a fast timescale characterized

by the phosphorylation rate $k_4 W_T \in [6, 600]$ min^{-1} [13]. The other phosphotransfer reactions evolve in a slower time scale since $\{k_5,\ k_7,\ k_8,\ k_9 p_T,\ k_{10} p_T,\ k_{11},\ k_{12} p_T\} \leq 0.02$ min^{-1} [15]. Also, the binding/unbinding reactions of x^* and x^{**} with DNA load promoter sites occurs at a maximum rate $k_{\text{on}} p_T \leq 0.13$ min^{-1} [15]. Thus, we can justify the application of singular perturbation theory with small parameter $\epsilon = \delta/(k_4 W_T)$. In particular, we define constants not depending on ϵ: $c_1 := k_1/k_4$, $c_2 := k_2/k_4$, $c_3 := k_3/k_4$, $c_5 := k_5/\delta$ $c_6 := k_6/(k_4 W_T)$, $c_7 := k_7/\delta$, $c_8 := k_8/\delta$, $c_9 := k_9 p_T/\delta$, $c_{10} := k_{10} p_T/\delta$, $c_{11} := k_{11}/\delta$, $c_{12} := k_{12} p_T/\delta$, $\kappa_p := k_p/(k_4 W_T)$, $\kappa_p' := k_p'/\delta$, $\alpha := X_T/W_T$, $\kappa_{\text{on}} := k_{\text{on}} p_T/\delta$, $\kappa_{\text{off}} := k_{\text{off}}(p_T/X_T)/\delta$, and $\epsilon_1 = p_T/X_T$. Defining $\bar{k}(t) := k(t)/Z_0$, system (9)-(15) becomes:

$$\dot{z}_T = \bar{k}(t) - \delta z_T \tag{16}$$

$$\begin{aligned}\epsilon \dot{z}^* =& -c_1 \delta z^*(1-w^*) + c_2 \delta w^*(z_T - z^*) + \kappa_p \delta (z_T - z^*) \\ & - \epsilon \kappa_p' \delta z^* - \epsilon \delta z^*\end{aligned} \tag{17}$$

$$\begin{aligned}\epsilon \dot{w}^* =& c_1 \delta \frac{Z_0}{W_T} z^*(1-w^*) - c_2 \delta \frac{Z_0}{W_T} w^*(z_T - z^*) \\ & - c_3 \alpha \delta \left(1 - x^{**} \boxed{-\epsilon_1 c^* - \epsilon_1 c^{**}}\right) w^* \\ & + \alpha \delta x^*(1-w^*) + \alpha \delta x^{**}(1-w^*) - \epsilon c_7 \delta w^* \\ & \overbrace{+\epsilon c_9 \delta c^* w^* + \epsilon c_{10} \delta c^{**}(1-w^*) + \epsilon c_{12} \delta c^*(1-w^*)}^{\bar{s}_1}\end{aligned} \tag{18}$$

$$\begin{aligned}\epsilon \dot{x}^* =& c_3 \delta \left(1 - 2x^* - x^{**} \boxed{-\epsilon_1 c^* - \epsilon_1 c^{**}}\right) w^* \\ & - \delta x^*(1-w^*) + \delta x^{**}(1-w^*) + c_6 \delta x^{**} - \epsilon c_5 \delta x^* \\ & \overbrace{-\epsilon \kappa_{\text{on}} \delta x^*(1-c^*-c^{**}) + \epsilon \kappa_{\text{off}} \delta c^*}^{\bar{s}_2}\end{aligned} \tag{19}$$

$$\begin{aligned}\epsilon \dot{x}^{**} =& c_3 \delta x^* w^* - c_6 \delta x^{**} - \delta x^{**}(1-w^*) \\ & \overbrace{-\epsilon \kappa_{\text{on}} \delta x^{**}(1-c^*-c^{**}) + \epsilon \kappa_{\text{off}} \delta c^{**}}^{\bar{s}_3}\end{aligned} \tag{20}$$

$$\begin{aligned}\dot{c}^* =& \kappa_{\text{on}} \delta \frac{X_T}{p_T} x^*(1-c^*-c^{**}) - \kappa_{\text{off}} \delta \frac{X_T}{p_T} c^* + c_8 \delta c^{**} \\ & - c_9 \delta \frac{W_T}{p_T} c^* w^* + c_{10} \delta \frac{W_T}{p_T} c^{**}(1-w^*) \\ & - c_{11} \delta c^* - c_{12} \delta \frac{W_T}{p_T}(1-w^*) c^*\end{aligned} \tag{21}$$

$$\begin{aligned}\dot{c}^{**} =& \kappa_{\text{on}} \delta \frac{X_T}{p_T} x^{**}(1-c^*-c^{**}) - \kappa_{\text{off}} \delta \frac{X_T}{p_T} c^{**} - c_8 \delta c^{**} \\ & + c_9 \delta \frac{W_T}{p_T} c^* w^* - c_{10} \delta \frac{W_T}{p_T} c^{**}(1-w^*).\end{aligned} \tag{22}$$

System (16) - (22) fits the structure of (1) - (4) with $u = z_T$, $x = (z^*, w^*, x^*, x^{**})^T$, $v = (c^*, c^{**})^T$. The dynamics of $u(t)$ are given by (14), the function vector $s = (\bar{s}_1, \bar{s}_2, \bar{s}_3)^T$ using the functions under braces in (18) - (20), and $\psi(v) = c^* + c^{**}$ which is bounded since both c^* and c^{**} are inside $[0, 1]$. Functions $f(u, x, \epsilon_1 \psi(v))$, $h(y, v)$ and matrices C, M and B can be defined by inspection. We will now focus on proving that assumption 4 in Theorem 1 holds, and assume all smoothness and uniqueness conditions are met.

Assumption 4): To prove that the slow manifold is locally exponentially stable, we verified that the Jacobian of the fast system with $\epsilon = 0$ given by $\frac{dx}{d\tau} = f(u, x, \epsilon_1 \psi(v))$ (where u and v are frozen in time and $\tau = t/\epsilon$) has eigenvalues with strictly negative real parts uniformly in z_T when (z^*, w^*, x^*, x^{**}) belong to the slow manifold ($\epsilon = 0$ in equations (17) - (20)). We numerically calculated the Jacobian of the system as a function of z_T and showed that the eigenvalues have strictly negative real part, as seen in Fig. 3, with the largest eigenvalue bounded above by -0.025.

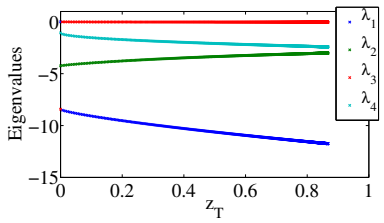

Fig. 3: The Jacobian of system $\frac{dx}{d\tau} = f(t, u, x, \epsilon_1 \psi(\bar{v}))$ was numerically calculated for varying normalized z_T concentrations. The systems eigenvalues have strictly negative real parts, with the slowest eigenvalue bounded above by -0.025. The parameter values considered for this and all simulations are: $k_{\text{on}} = 6$, $k_{\text{off}} = 0.0138$, $p_T = 0.0220$, $\delta = 0.0065$, $k_p = 0.9033$, $k_p' = 0.0533$, $k_1 = 500.19$, $k_2 = 1.26 \times 10^3$, $k_3 = 478.85$, $k_4 = 60.00$, $k_5 = 0.01$, $k_6 = 0.6948$, $k_7 = 0.01$, $k_8 = 0.0047$, $k_9 = 0.0858$, $k_{10} = 0.7827$, $k_{11} = 0.0073$, $k_{12} = 0.5$, $X_T = 0.0712$, $W_T = 0.1752$ as reported in [15]. All concentration units are in [μM] and time units are in [min].

Hence by Theorem 1 we have that system (16) - (22) works as an insulation device employing the principle of timescale separation. The insulation device retroactivity attenuation dependence on fast internal dynamics is depicted in Fig. 4. Here we see that the retroactivity attenuation is decreased as the parameters providing the fast internal timescale are decreased. This is consistent with the requirement of a small $\epsilon = \delta/(k_4 W_T)$.

IV. Sensitivity Analysis

To further explore how the retroactivity attenuation property depends on the internal parameters of the system, we performed a sensitivity analysis on the insulation device output. Specifically, we expect that uniform decrease in the parameters $\{W_T k_1, W_T k_2, W_T k_3, W_T k_4, k_6\}$ controlling the insulation device's timescale will worsen retroactivity attenuation.

For a general state equation $\dot{\mathbf{x}} = f(t, \lambda)$, continuous in $(t, \mathbf{x}, \lambda)$ and with continuous first partial derivatives on the set of internal parameters λ, we can define the sensitivity of a state trajectory $\mathbf{x}(t, \lambda)$ to parameters λ by taking the partial derivative with respect to λ [12]. This is given by:

$$S_\lambda(t, \lambda) = \frac{\partial}{\partial \lambda} x(t, \lambda), \tag{23}$$

which is a matrix in $\mathbb{R}^{\text{nxp}}$, where n is the number of states and p is the number of parameters in λ. By defining the Jacobian matrices:

$$J_1(t, \lambda) := \frac{\partial f(t, x, \lambda)}{\partial x}, \quad J_2(t, \lambda) := \frac{\partial f(t, x, \lambda)}{\partial \lambda},$$

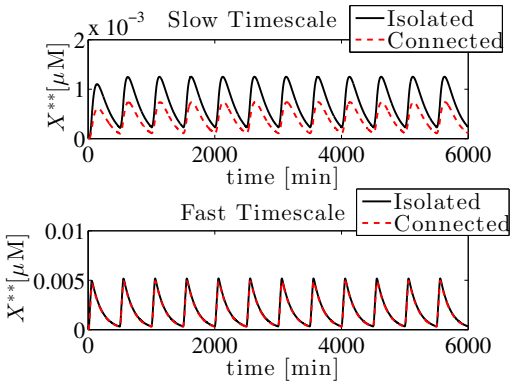

Fig. 4: The Slow Timescale simulation denotes the output level X^{**} of (9) - (15) in both isolated, $p_T = 0$, and connected, $p_T \neq 0$ systems when the phosphorylation rate constants $\{k_1, k_2, k_3, k_4, k_6\}$, considered as the fast reactions in system (9) - (15), are reduced to 10% of their nominal value given in Fig. 3. The Fast Timescale simulation shows the output X^{**} for the original parameter values given in Fig. 3. The considered input $k(t)$ was a periodic square wave with on-time of 50 minutes and period of 500 minutes with magnitude of 1×10^{-4}[μM/min].

we can write the differential equation for the sensitivity matrix as

$$\dot{S}_\lambda = J_1(t, \lambda_0) S_\lambda(t) + J_2(t, \lambda_0), \tag{24}$$

where matrices J_1 and J_2 are evaluated at the nominal trajectory $\mathbf{x}(t, \lambda_0)$ and parameter values λ_0. In our case we have $\mathbf{x} = (Z^*,\ W^*,\ X^*,\ X^{**},\ C^*,\ C^{**})^T$ and $\lambda = (\delta,\ k_p,\ k_p,\ k_1,\ k_2,\ k_3,\ k_4,\ k_5,\ k_6,\ k_7,\ X_T,\ W_T)^T$ with nominal parameter values λ_0 as given in Fig. 3. Defining the diagonal matrix $D_\lambda := \text{diag}\{\lambda_1, \lambda_2, \ldots, \lambda_n\}$, we can obtain the normalize sensitivity $\bar{S}_\lambda = S_\lambda D_\lambda$. The normalize sensitivity can be seen as the concentration change of species $\mathbf{x_i}$ due to a percentile change in the individual parameter λ_i, which allows for sensitivity comparison between parameters of different nature.

We define the output error as the squared difference between the unloaded output trajectory X^{**} and loaded output trajectory X_L^{**}, $e_y(t, \lambda) := (X^{**}(t, \lambda) - X_L^{**}(t, \lambda))^2$, where the unloaded system has $p_T = 0$ in (12) - (15) and the loaded system has $p_T \neq 0$. This allows to assess the sensitivity of the retroactivity attenuation property to parameters λ, since we are directly comparing the behavior of the insulation device in isolation and to that when connected. This sensitivity is given by:

$$\frac{\partial e_y(t, \lambda)}{\partial \lambda} = 2[X^{**}(t, \lambda) - X_L^{**}(t, \lambda)][\bar{S}_\lambda(t, \lambda) - \bar{S}_\lambda^L(t, \lambda)], \tag{25}$$

where $\bar{S}_\lambda$ and $\bar{S}_\lambda^L$ denote the normalized unloaded and loaded output sensitivities respectively. The simulation results of the normalized output error sensitivity are given in Fig. 5 for periodic square wave input with a fixed on-time of 50 minutes and period of 500 minutes.

In this analysis, an increase in the squared error is given by positive error sensitivity while a decrease in the squared error is given by negative error sensitivity. From Fig. 5 (c), we can see that the output error performance is highly sensitive to the total phosphatase concentration W_T and the X^{**} dephoshorylation rate k_6. Increasing these parameters leads to an improvement in the insulation device's performance, consistent with having $\epsilon \ll 1$ in Theorem 1. We can also see from Fig. 5 (a) that the output error is sensitive to parameter k_p which has positive sensitivity. Looking at Z^* as the input to the YPD1/SKN7 cascade, the Z^* phosphorylation rate k_p leads to an increase in the insulation device driver signal. This, in turn, increases the formation of C^* and C^{**}, worsening the approximation of x with $\gamma_0(t)$ from Theorem 1 (since it is no longer true that $\epsilon_1 \psi(v) \ll 1$) by making the output X^{**} dependent on C^* and C^{**}. The results of the sensitivity analysis are consistent with the assumption that $\epsilon = \delta/(W_T k_4)$ is small in a neighborhood of λ to allow for retroactivity to the output attenuation through separation of timescales as described in Theorem 1.

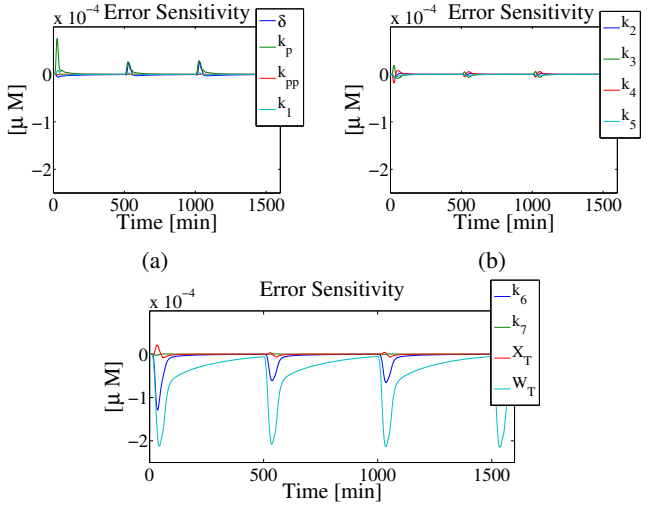

Fig. 5: The error sensitivity given in (25) was calculated from the normalized dynamic sensitivities and output trajectory of both loaded and unloaded insulation devices.

V. Retroactivity Attenuation Performance

The timescale and sensitivity analysis presented thus far motivates further study of the insulation devices output error dependence on both internal dynamic timescale and individual tunable parameters X_T and W_T. This was explored by simulating the unloaded and loaded insulation device using the same input signal with a fixed on-time of 50 minutes and period of 500 minutes, and calculating the mean squared output error given by (26) for changes in phosphorylation timescale and protein concentrations X_T, W_T:

$$E = \frac{1}{T} \int_0^T \left[\frac{X^{**}(t) - X_L^{**}(t)}{\max[X^{**}(t)]} \right]^2 dt. \tag{26}$$

Changes in timescale illustrate how the underlying principle of timescale separation allows for retroactivity attenuation. Furthermore, concentrations X_T and Y_T are the physical

tunable parameters in the system since reaction timescale cannot be easily modulated experimentally. Thus their relation to the retroactivity attenuation property is important for the insulation device's practical implementation.

A. Retroctivity attenuation dependence on timescale

The insulation device performance dependence on timescale was evaluated by simulating the normalized system (16) - (22) after modulating the parameter $1/\epsilon$ in (17) - (20). Increasing $1/\epsilon$ leads to faster timescale while decreasing this parameter leads to a slow down in the insulation devices timescale. The output error performance was assessed by calculating the mean squared error in (26) across a range of promoter sites p_T, which controls the amount of load placed on the insulation device. The parameter ratio $\epsilon_1 = p_T/X_T$ was kept constant across all simulations by increasing X_T proportionally to p_T. This prevents from changes in the slow manifold of system (16) - (22).

We can see from the simulation results shown in Fig. 6 (a)-(d) that the error increases with the amount of promoter sites for a constant $1/\epsilon$. This is expected since an increase in p_T leads to a higher effect of the retroactivity fluxes $\bar{s}_1$, $\bar{s}_2$ $\bar{s}_3$ on the (16) - (22) system dynamics. On the other hand, the mean squared error is decreased for an increase in parameter $1/\epsilon$. This implies that the insulation device is able to attenuate higher retroactivity effects as the timescale of the internal processes becomes faster. Also, form Fig. 6 (c)-(d) we see that the mean squared error is increased as the timescale of the phosphotransfer reactions is slowed to the extent of the degradation processes. These simulations reveal that the fast internal dynamics of the insulation device indeed allows for retroactivity attenuation, while slow internal dynamics harms this property.

B. Retroactivity attenuation dependence on the total substrate and phosphatase concentration

System (9) - (15) was simulated assuming $\alpha = X_T/W_T$ is kept constant by increasing proportionally concentrations X_T and W_T. The error due to an increase in the p_T promoter sites concentration was assessed using expression (26). As in part A. we see that the error increases as the amount of promoter sites p_T is increase, which is shown in Fig. 7 (a)-(d). Also, the error is reduced as the concentrations X_T and W_T are increased for all values of load. This is in accordance with the fact that these two factors are directly related to the retroactivity attenuation property of the insulation device as described in Section III.

Having high X_T prevents from changes in steady state of system (9) - (15) due to the load by making $\epsilon_1 \ll 1$. Furthermore, in the case where the reactions with timescale $k_1 W_T$, $k_2 W_T$, $k_3 W_T$, and $k_4 W_T$ are rate limiting (or slowest), increasing W_T improves the approximation $\epsilon \approx 0$, as it follows from the definition of ϵ given in Section III. On the other hand, decreasing both X_T and W_T concentrations have adverse effects on the insulation devices output error as seen in Fig. 7 (c)-(d). This means that the retroactivity attenuation property requires a minimal concentration X_T and W_T for its successful implementation.

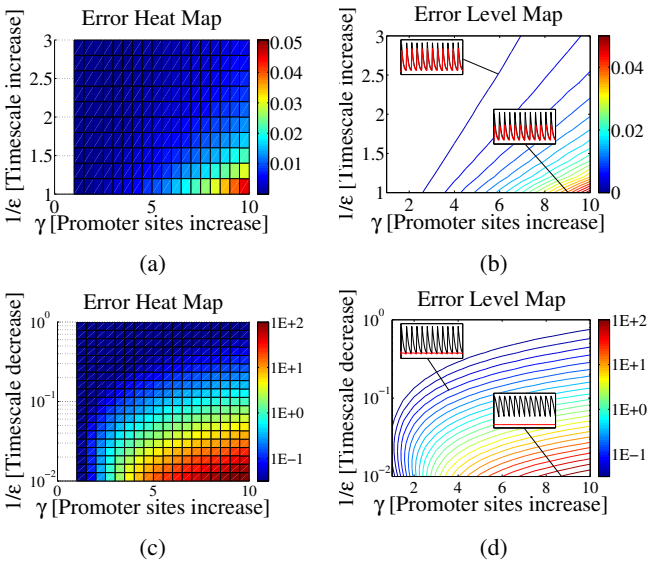

Fig. 6: In this simulation the constant G represents the increase in timescale (a)-(b) or decrease of timescale (c)-(d) of the internal insulation device phosphotransfer reactions. It reports the error (26) for the simulated system (16) - (22) with varying promoter site concentrations $p_T = \gamma p_T^0$ where p_T^0 is the total promoter site concentration given in Fig. 3.

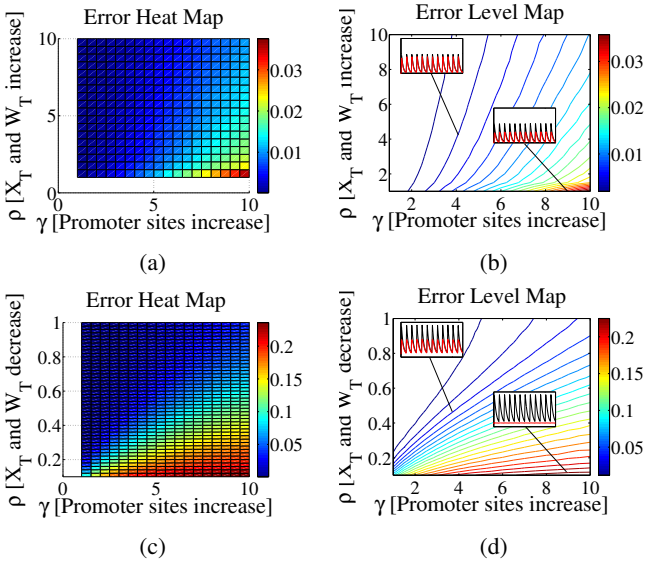

Fig. 7: In these simulations, ρ provides the fold increase or decrease in the total SKN7 concentration X_T and YPD1 concentration W_T. The reported error was calculated applying (26) for the simulated system (9) - (15), with promoter sites concentrations given by $p_T = \gamma p_T^0$ where p_T^0 is the total promoter site concentration given in Fig. 3.

VI. Conclusions and future work

This work demonstrates that the natural phosphotransfer YPD1/SKN7 cascade works as an insulation device by employing the principle of timescale separation for retroactivity attenuation. This was validated through a singular perturbation analysis, which showed that the fast nature of phosphotransfer reactions allows for the insulation device's dynamics to be decoupled from the load, in the case the cycle substrate is in sufficient amount. This finding was further validated through a sensitivity analysis in which it was shown that increasing the concentration W_T and the spontaneous dephosphorylation rate k_6 leads to a reduction in the insulation device output error. It was demonstrated through simulation that reducing the phosphotransfer reaction timescale diminishes the retroactivity attenuation property, and that the physical tunable parameters of the system (substrate concentration X_T and phosphatase concentration W_T) could be modulated to enhance retroactivity attenuation. This result allows for the implementation of signal transduction cascades as insulation devices due to the fast nature of protein/protein interactions. Our results highlight a new role that cascades of fast phosphotranfer reactions may play in natural networks and suggest that they can be employed as insulation devices in synthetic biology to enable modular composition. All the theoretical predictions described in this work were experimentally validated by Deepak *et al.*[15], providing real evidence of the insulation device performance in synthetic circuits. Future work includes the implementation of insulation devices to interconnect functional signaling systems.

References

[1] L. H. Hartwell, J. J. Hopfield, S. Leibler, and A. W. Murray. From molecular to modular cell biology. *Nature*, 402:C47–C52, 1999.

[2] N. Kashtan and U. Alon. Spontaneous evolution of modularity and network motifs. *Proceedings of the National Academy of Sciences of the United States of America*, 102(39):13773–13778, 2005.

[3] P. EM Purnick and R. Weiss. The second wave of synthetic biology: from modules to systems. *Nature Reviews Molecular Cell Biology*, 10(6):410–422, 2009.

[4] S. A. Benner and A. M. S. Synthetic biology. *Nature Reviews Genetics*, 6(7):533–543, 2005.

[5] S. Cardinale and A. P. Arkin. Contextualizing context for synthetic biology–identifying causes of failure of synthetic biological systems. *Biotechnology journal*, 7(7):856–866, 2012.

[6] D. Del Vecchio, A. J. Ninfa, and E. D. Sontag. Modular cell biology: retroactivity and insulation. *Molecular systems biology*, 4(161):161, January 2008.

[7] J. Saez-Rodriguez, S. Gayer, M. Ginkel, and E. D. Gilles. Automatic decomposition of kinetic models of signaling networks minimizing the retroactivity among modules. *Bioinformatics (Oxford, England)*, 24(16):i213–9, August 2008.

[8] Y. Kim, Z. Paroush, K. Nairz, E. Hafen, G. Jiménez, and S. Y. Shvartsman. Substrate-dependent control of mapk phosphorylation in vivo. *Molecular systems biology*, 7(1), 2011.

[9] P. Jiang, A. C. Ventura, E. D. Sontag, S. D. Merajver, A. J. Ninfa, and D. Del Vecchio. Load-induced modulation of signal transduction networks. *Science signaling*, 4(194):ra67, 2011.

[10] S. Jayanthi, K. S. Nilgiriwala, and D. Del Vecchio. Retroactivity controls the temporal dynamics of gene transcription. *ACS Synthetic Biology*, 2(8):431–441, 2013.

[11] S. Jayanthi and D. Del Vecchio. Retroactivity attenuation in biomolecular systems based on timescale separation. *Automatic Control, IEEE Transactions on*, 56(4):748–761, 2011.

[12] H. K. Khalil. *Nonlinear systems*. Prentice-Hall, Upper Saddle River, NJ, 2002.

[13] E. Klipp, B. Nordlander, R. Krüger, P. Gennemark, and S. Hohmann. Integrative model of the response of yeast to osmotic shock. *Nature biotechnology*, 23(8):975–982, 2005.

[14] J. E. Marsden and M. J. Hoffman. Elementary classical analysis. *W. H Freeman and Company*, 1993.

[15] D. Mishra, P. M. Rivera-Ortiz, A. Lin, D. Del Vecchio, and R. Weiss. A load driver device for engineering modularity in biological networks. *Science*, 2013 to appear.

[16] A. Belle, L. Tanay, A.and Bitincka, and E. K. Shamir, R.and O'Shea. Quantification of protein half-lives in the budding yeast proteome. *Proceedings of the National Academy of Sciences of the United States of America*, 103(35):13004–9, August 2006.